

**MINIMIZING THE CURRENT HARMONICS RMS VALUE OF THREE-PHASE
PWM CONVERTER SYSTEMS BY OPTIMAL AND SUBOPTIMAL TRANSITION
BETWEEN CONTINUOUS AND DISCONTINUOUS MODULATION**

JOHANN W. KOLAR, HANS ERTL, FRANZ C. ZACH
Technical University Vienna, Power Electronics Section, Gusshausstrasse 27,
Vienna, AUSTRIA

Phone: (int)43 222 58801-3886 Fax: (int)43 222 5052666

Abstract

A given converter voltage space vector can be realized by a three-phase PWM converter system by switching only two bridge legs. There, the third phase is clamped to the positive or negative DC link voltage. This method is called *discontinuous modulation* due to the discontinuous shape of the generating phase modulation functions. (On the contrary, *continuous modulation* is given in the case where all bridge legs are switched. The phase modulation functions are continuous in this case.) As a closer analysis shows, the discontinuous method allows to increase the effective system pulse frequency, dependent on the phase angle between converter output voltage and output current. There, the basis for a comparison with the continuous method is chosen as equal average switching losses of any converter bridge leg. Therefore, there result operating regions where the quality index (defined by the harmonic losses) for discontinuous modulation is significantly beneath the index for continuous modulation.

For harmonic-optimal operation therefore one has to change between continuous and discontinuous modulation (or between various variants of the discontinuous modulation) in dependency on the load status. The harmonic losses of the control methods are calculated directly in the time domain. For this purpose, the space vector calculus is applied and approximations are used which are sufficiently exact for PWM converter systems with high pulse frequency.

Besides the determination of the exact limits of the operating regions of the various modulation methods the paper also discusses suboptimal approximations of these limits for the application of the system as PWM rectifier, static Var compensator or machine converter.

According to the duality relationships between DC voltage link and DC current link PWM converters all control (modulation) methods described here can be directly transferred to the DC current link converter.

Keywords: Three-Phase DC Voltage Link Inverter/Rectifier System, Space Vector Calculus, Current Harmonics RMS Value, Pulse Pattern Optimization, Continuous Modulation, Discontinuous Modulation.

1 Introduction

In the following the mathematical formulation of the voltage generation and of the the harmonic losses is described. Also, a summary of the optimization of the continuous modulation and the basics of the discontinuous modulation are given. Then a detailed analysis of the methods for controlling a three-phase PWM converter system with DC voltage link (cf. Fig.1) based on discontinuous modulation is presented (cf. also Ref.[1], Ref.[2], Ref.[3]).

There, exclusively the converter operation without overmodulation is considered. Furthermore, pulse frequencies are assumed which are sufficiently higher than that of the output voltage fundamental. This allows analytically closed calculations and therefore results in simple mathematical expressions for the characteristic quantities of the modulation methods.

2 Space Vector Calculus and Voltage Generation

Due to the floating mains/load neutral point the representation of the converter voltage system can be given via the related space vector

$$\underline{u}_U = \frac{2}{3} [u_{U,R} + a u_{U,S} + a^2 u_{U,T}] \quad a = \left(-\frac{1}{2} + j\frac{\sqrt{3}}{2}\right) \quad (1)$$

There, the phase voltages $u_{U,R}$, $u_{U,S}$ and $u_{U,T}$ shall be referenced to the center point of the DC link voltage. The zero-quantity

$$u_0 = \frac{1}{3}(u_{U,R} + u_{U,S} + u_{U,T}) \quad (2)$$

(which is decoupled due to the space vector transformation) characterizes a voltage contribution which at a given time appears equally in all converter phase voltages. This contribution defines the voltage between mains/load

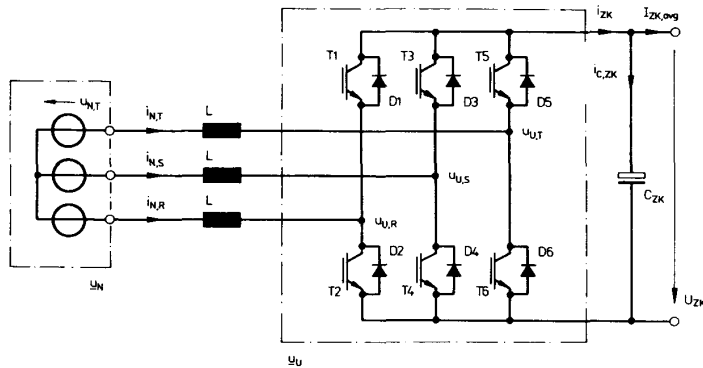


Fig.1: Structure of the power circuit of a three-phase voltage DC link PWM converter system. For usage as *PWM inverter* for AC machine drives the inductances L and the three phase system \underline{u}_N can be interpreted as simple equivalent circuit of the AC machine formed by leakage inductances and machine counter emf. On the other hand, for mains operation of the *PWM converter* (PWM rectifier, static Var compensator) the inductances have to be connected in series; the voltage system \underline{u}_N is defined by the mains conditions.

neutral point and DC link voltage center point for the case of a mains/load voltage system without zero quantities. Furthermore, this contribution does not influence the generation of the output currents.

According to Eq.(1) the sinusoidal converter voltage system to be generated is described by

$$\underline{u}_U^* = \hat{U}_U^* \exp j\varphi_U \quad \varphi_U = \omega_N \tau. \quad (3)$$

For the definition of the modulation depth we have

$$M = \frac{2\hat{U}_U^*}{U_{ZK}} \quad M \in [0, \frac{2}{\sqrt{3}}]. \quad (4)$$

For the further considerations we can assume that the converter bridge legs are replaced by two-pole switches between positive and negative DC link voltage bus. If we relate a two-level switching function to each bridge leg according to

$$\begin{aligned} u_{U,R} &= +\frac{1}{2}U_{ZK} & s_{P,R} &= 1 \\ u_{U,R} &= -\frac{1}{2}U_{ZK} & s_{P,R} &= 0 \end{aligned} \quad (5)$$

we can denote each of the 8 possible converter switching states by a binary number ($s_{P,R}, s_{P,S}, s_{P,T}$)₂ (which is formed based on the instantaneous values of the switching functions) or by its decimal equivalent.

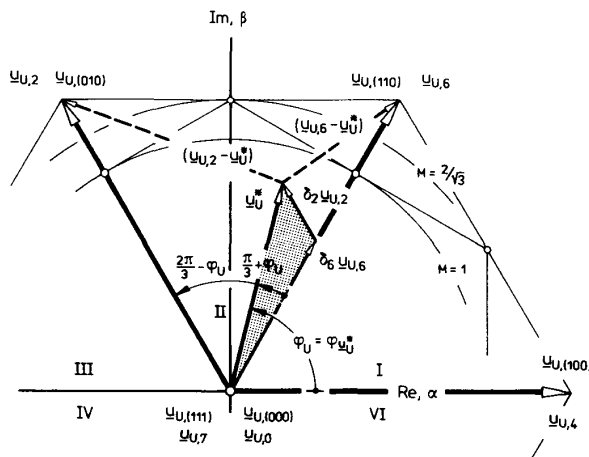
Due to the 60°-symmetry of the converter voltage space vectors resulting for the various converter switching states (except the free-wheeling states (000), (111)) the considerations in the following are limited to the angle interval $\varphi_U \in [\frac{\pi}{3}, \frac{2\pi}{3}]$. As Fig.2 shows, in the angle interval considered, a particular output voltage space vector \underline{u}_U^* is formed regarding its time average over a pulse half-period $\frac{1}{2}T_P$ by a switching state sequence

$$\varphi_U \in [\frac{\pi}{3}, \frac{2\pi}{3}] \quad \dots 0 \ 2 \ 6 \ 7 \Big|_{t_\mu=0} \ 7 \ 6 \ 2 \ 0 \Big|_{t_\mu=\frac{T_P}{2}} \ 0 \ 2 \ 6 \ 7 \dots \quad (6)$$

For defining the switching states we have here, accordingly to the previously made remarks,

$$\begin{aligned} [111]_2 &= 7_{10} \\ [110]_2 &= 6_{10} \\ [010]_2 &= 2_{10} \\ [000]_2 &= 0_{10}. \end{aligned} \quad (7)$$

The switching state sequence is selected regarding minimal switching frequency such that switching of only one bridge leg leads to the following converter voltage space vector. This explains the order of the switching states in alternating increasing and decreasing sequence (cf. Eq.(6)). The variable t_μ denotes a local (microscopic) time within the pulse periods. The position of the pulse interval within the fundamental period is defined by the angle φ_U or by the global (macroscopic) time τ . For the (relative) duration of the switching states related to one pulse half-period there follows



$$\begin{aligned} \delta_6 &= \frac{\sqrt{3}M}{2} \sin\left(\varphi_U + \frac{\pi}{3}\right) \\ \delta_2 &= \frac{\sqrt{3}M}{2} \sin\left(\varphi_U - \frac{\pi}{3}\right) \\ \delta_0 + \delta_7 &= 1 - (\delta_2 + \delta_6). \end{aligned} \quad (8)$$

$$(9)$$

3 Space Vector of the Output Current Harmonics

The calculation of the output current harmonics

$$\Delta \underline{i}_N = \underline{i}_N - \hat{\underline{i}}_N^* \quad (10)$$

existing due to the way of generating a given output voltage space vector \underline{u}_U^* (which is only possible in the average over a pulse period) can now be performed directly in the time domain. There, a sufficiently high pulse number $p_z = T_N/T_P = f_P/f_N$ is assumed (T_N ...fundamental period, T_P ...pulse period, f_N and f_P are the related frequencies). The ideally to be generated output current space vector shall be given by

$$\hat{\underline{i}}_N^*(\tau) = \hat{I}_N^* \exp j(\omega_N \tau + \varphi) \quad \varphi = \varphi_{\underline{u}_U^*, \hat{\underline{i}}_N^*}. \quad (11)$$

For a harmonic-free mains voltage system the output current harmonics are defined directly based on the integral of the local deviation between the reference value and the actually generated converter voltage. For approximation of the circular trajectory of the output current fundamental space vector by the local tangent in the instant τ (macroscopic position of the considered pulse interval) the space vector $\Delta \underline{i}_N$ of the current harmonics describes a trajectory within a pulse half-period as shown in Fig.3, starting and ending in the origin of the coordinate system.

The ratio of the sides of the triangle giving the current deviations are determined like the relative switching state time intervals (cf. Eqs.(8), (9)) directly by modulation depth M and phase angle φ_U of the converter voltage space vector to be generated. However, there is nothing said about the split of the free-wheeling state between beginning and end of each pulse half-interval. This represents a parameter for optimising the modulation method regarding the harmonics.

4 Harmonic-Optimal Continuous Modulation

If one chooses the rms value of the current harmonics as quality factor (to be minimized by an optimal converter control) according to

$$\begin{aligned} \Delta I_{N,rms}^2 &= \frac{1}{3T_N} \int_{T_N} \left\{ \frac{2}{T_P} \int_{t_\mu=0}^{t_\mu=\frac{T_P}{2}} (\Delta i_{N,R}^2 + \Delta i_{N,S}^2 + \Delta i_{N,T}^2) dt_\mu \right\} d\tau \\ &= \frac{1}{3T_N} \int_{T_N} \Delta i_{N,RST,rms}^2(\tau) d\tau \rightarrow Min \end{aligned} \quad (12)$$

(approximation for high pulse number), one can include the considerations made in section 3 directly into the optimization procedure. A minimization of the phase-related global harmonic losses has to be performed according to Eq.(12) by minimizing the (always positive) power loss contributions of the single pulse intervals. Then the optimization can be performed separately for each pulse interval based on a quality factor

$$\Gamma = \Delta i_{N,RST,rms}^2(\tau) \rightarrow Min. \quad (13)$$

Fig.2: Basically there can be generated only such output voltage space vectors \underline{u}_U^* which lie within the equilateral triangle formed by the converter voltage space vectors $\underline{u}_{U,2}$ and $\underline{u}_{U,6}$. The margin in direction to overmodulation therefore is given (if the generation of a sinusoidal output voltage system is required) by $M = \frac{2}{\sqrt{3}}$ (as shown); parameters of \underline{u}_U^* : $M = 0.75$, $\varphi_U = 75^\circ$.

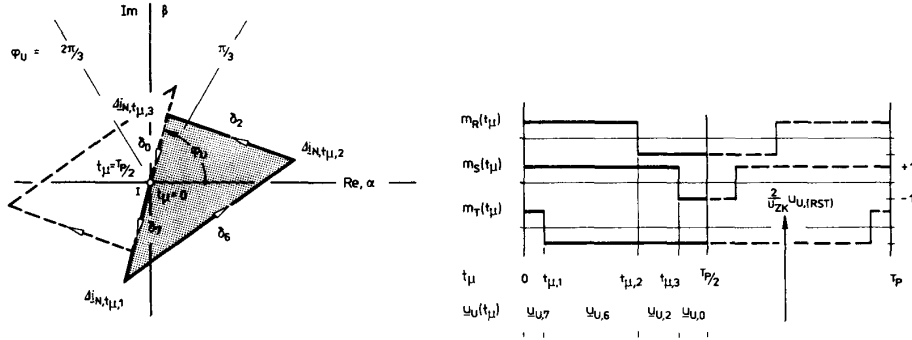


Fig. 3: Trajectory of the harmonic currents space vector Δi_N within a pulse half-period; right side: microscopic time behavior of the related normalized converter voltages (pulse pattern). The non-voltage-forming free-wheeling state is realized alternating by the switching states (000) and (111); according to continuous modulation it is split up between beginning and end of each pulse half-period; parameters: $M = 0.75$, $\varphi_U = 75^\circ$.

(which can be defined as local harmonic current rms value). In Eq.(13) the sum of the phase contributions is denoted by RST. Equation (13) is directly related to the trajectory of the harmonic currents space vector Δi_N by

$$\Delta i_{N,RST,rms}^2(\tau) = \frac{1}{3T_P} \int_{t_\mu=0}^{t_\mu=T_P/2} |\Delta i_N(t_\mu)|^2 dt_\mu. \quad (14)$$

Comparison with concepts from mechanics shall illustrate the considerations made here: Equation (14) has a similarity to the definition of a 2nd order moment of inertia of a mass distribution (in this case there is the analogy to the harmonic current space vector trajectory which is considered having mass) related to an axis leading through the "bearing point" I of the harmonic current triangle. (The "bearing point" I (see Fig.3) lies in the origin.)

Then the optimisation problem is clearly analogous to the problem to shift the harmonic triangle by appropriate distribution of the free-wheeling states 0, 7 such that a minimisation of the "moment of inertia" is achieved. In the course of the actual calculation we have to consider, however, a time-weighting (δ_7 , δ_6 , δ_2 , δ_0) of the single trajectory segments. This goes beyond the analogy described.

For the local harmonic current rms value we receive after an involved calculation

$$\Delta i_{N,RST,rms}^2(\tau) = \Delta i_{N,RST,rms,1}^2\{\delta_7(\tau), \delta_6(\tau), \delta_2(\tau)\} + i_{N,RST,rms,2}^2\{\delta_6(\tau), \delta_2(\tau)\} \quad (15)$$

$$\begin{aligned} \frac{1}{\Delta i_n^2} \Delta i_{N,RST,rms,1}^2 &= \frac{48}{9} \delta_7 \left\{ \delta_2 \delta_6 (\delta_2 - \delta_6) - 2\delta_{26} [1 - (\delta_7 + \delta_6 + \delta_2)] \right\} \\ \frac{1}{\Delta i_n^2} \Delta i_{N,RST,rms,2}^2 &= \frac{16}{9} \left\{ 6\delta_{26}^2 + 2\delta_{26} - 4\delta_2^4 - 4\delta_6^4 - 4\delta_2\delta_{26} - 4\delta_6\delta_{26} - \right. \\ &\quad \left. - 8\delta_2\delta_6\delta_{26} + 2\delta_2\delta_6^2 - \delta_2^2\delta_6 + 3\delta_2^3\delta_6 - \delta_2^2\delta_6^2 \right\} \quad (16) \end{aligned}$$

with

$$\delta_{26} = \delta_2^2 + \delta_2\delta_6 + \delta_6^2 \quad (17)$$

$$\Delta i_n = \frac{U_{2K} T_P}{8L}. \quad (18)$$

The optimisation of the harmonic current losses of the modulation method (cf. Eq.(12)) therefore is reduced to the solution of a simple extremal value problem

$$\frac{\partial}{\partial \delta_7} \Delta i_{N,RST,rms,1}^2 \Big|_{\delta_7, \Gamma = \min} = 0. \quad (19)$$

The free-wheeling state interval δ_7 therefore leads under consideration of Eq.(8) and Eq.(9) or

$$\frac{\delta_7}{\delta_0} = \frac{\delta_7}{1 - (\delta_7 + \delta_6 + \delta_2)} \quad (20)$$

directly to the optimal distribution of the free-wheeling states.

In this paper we only want to discuss briefly the suboptimal solution of the optimisation calculus

$$\varphi_U \in \left[\frac{\pi}{3}, \frac{2\pi}{3} \right] \quad \delta_{0,[2]} = \delta_{7,[2]} = \frac{1}{2} [1 - (\delta_2 + \delta_6)] \quad (21)$$

which in the following will be used as characteristic example of continuous modulation.¹

The modulation method corresponding to Eq.(21) (as also given in Ref.[4], where it is called optimal, however) shows advantages regarding its practical realisation. This is due to the free-wheeling state distribution which is independent of φ_U and shows equal parts at the beginning and at the end of each pulse half-interval. As compared to the optimal solutions (cf. Refs.[2],[5]) there result only marginally higher harmonic losses. Furthermore, the voltage region up to the theoretical overmodulation limit ($M = \frac{2}{\sqrt{3}}$) can be used, as opposed to the optimal solution ($M \leq 0.972 \frac{2}{\sqrt{3}}$).

Further methods (known from the literature, cf. Refs.[6],[7]) which are based on the extension of simple sinusoidal modulation by addition of phase voltage harmonics of the order $3N$ show no substantial differences regarding the modulation limit (limit to overmodulation) and regarding the harmonics conditions. Therefore, a more detailed discussion shall be omitted here; the reader shall be referred to Ref.[5].

For the global harmonic losses (as used later for a comparison of various modulation methods) of the modulation method defined by Eq.(21) and denoted as [2]² in the following, there follows under consideration of Eqs.(12), (15), (16), (17), (18) and (21)

$$\Delta I_{N,rms,[2]}^2 = \frac{1}{6} \Delta i_n^2 M^2 \left[1 - \frac{8M}{\sqrt{3}\pi} + \frac{9M^2}{8} \left(1 - \frac{3\sqrt{3}}{4\pi} \right) \right]. \quad (23)$$

In general, the denomination of the modulation methods in this paper is based on other papers of the authors in the area "Harmonics Optimisation of Modulation Methods of Three-Phase PWM Converters" (cf. Refs.[1], [2], [3], [5]). Therefore the denomination is purposely not in the sequence as treated in this paper in order to make comparisons with earlier papers easier.

5 Discontinuous Modulation

If (contrary to the previously analysed (sub)optimal free-wheeling state distribution) the whole free-wheeling interval is shifted according to

$$\varphi_U \in \left[\frac{\pi}{3}, \frac{2\pi}{3} \right] \quad \dots 2 \ 6 \ 7 \Big|_{t_\mu=0} \ 7 \ 6 \ 2 \Big|_{t_\mu=\frac{T_P}{2}} \ 2 \ 6 \ 7 \dots \quad (24)$$

¹Continuous modulation shall be given when according to a switching sequence

$$\varphi_U \in \left[\frac{\pi}{3}, \frac{2\pi}{3} \right] \quad \dots 0 \ 2 \ 6 \ 7 \Big|_{t_\mu=0} \ 7 \ 6 \ 2 \ 0 \Big|_{t_\mu=\frac{T_P}{2}} \ 0 \ 2 \ 6 \ 7 \dots \quad (22)$$

within each pulse half-period all converter bridge legs are switched. The control signals then can be thought to be derived from continuous phase modulation functions. Therefore there occur always both free-wheeling states (000) and (111) of the converter system (cf. Fig.3, left hand side; beginning and end of the pulse half-period) in the switching sequence.

²Brackets denote modulation methods in this paper; references are marked, e.g., as Ref.[2].

to the beginning (in the following denoted as modulation method [6]) or, according to

$$\varphi_U \in \left[\frac{\pi}{3}, \frac{2\pi}{3} \right] \dots 0 \ 2 \ 6 \left|_{t_\mu = 0} \ 6 \ 2 \ 0 \right|_{t_\mu = \frac{T_p}{2}} \ 0 \ 2 \ 6 \dots \quad (25)$$

to the end (modulation method [7]) of the pulse half-period considered ($t_\mu \in [0, \frac{1}{2}T_p]$), we receive increased current harmonics and harmonic losses as compared to the optimal solution. (This can be explained clearly again by using the then higher "moment of inertia" of the harmonic current triangle (the "bearing" is in either of the corner points; see Figs.4 and 5, cf. also Fig.3).

An analysis of the switching state sequences given by Eqs.(24), (25) shows that the voltage generation in this case is performed by switching only two bridge legs where the third phase is "clamped" to the positive or negative DC link voltage bus (cf. Fig.4 - clamping of phase S to $+\frac{1}{2}U_{ZK}$ and Fig.5 - clamping of phase T to $-\frac{1}{2}U_{ZK}$).

Therefore, the line-to-line voltages are generated directly. This is opposed to the case of continuous modulation (switching of all bridge legs) which is based on phase voltages related to the DC link voltage center point. Considering the cyclic change of the clamping states between the phases (symmetry of the generated three-phase system), as a result each bridge leg is not pulsed within a third of the output voltage fundamental. If we assume equal average switching losses as for continuous modulation, this makes possible an increase of the (effective) system pulse frequency (cf. section 6) defined by a factor

$$k_{f,[i]} = \frac{f_{P,[i]}}{f_P} \quad (26)$$

(f_P ... pulse frequency for continuous modulation). This results accordingly in a reduction of the initially increased local harmonic loss contributions (which are caused by the shift of the free-wheeling states). (A pulse-frequency-proportional reduction of the linear dimensions of the current harmonics triangle results.) This motivates a closer analysis of discontinuous modulation methods³ and a comparison with continuous modulation.

Basically, a comparison of different modulation methods can be made on the basis of local and of global parameters. A local comparison (of each pulse period) is related to the concept of the local harmonic loss contribution (cf. Eq.(14)) as introduced for optimising the continuous modulation. For a comparison related to the fundamental we have to apply the (global) current harmonics rms value (cf. Eq.(12)).

At this location (cf. Fig.6) we want to add the dependency of the normalized local harmonic losses $\Delta_{N,RST,rms,[i]}^2$ on the modulation index and on the

³If within each pulse half-period only two bridge legs are switched (i.e., the free-wheeling state is not split up between beginning and end of the pulse half-period), this case shall be called *discontinuous modulation* in the following. The reason is that in this case the modulation signals of the bridge legs can be assumed to be derived from an intersection of a triangular carrier signal (with pulse frequency) with discontinuous phase modulation functions (cf. Refs.[1], [9]).

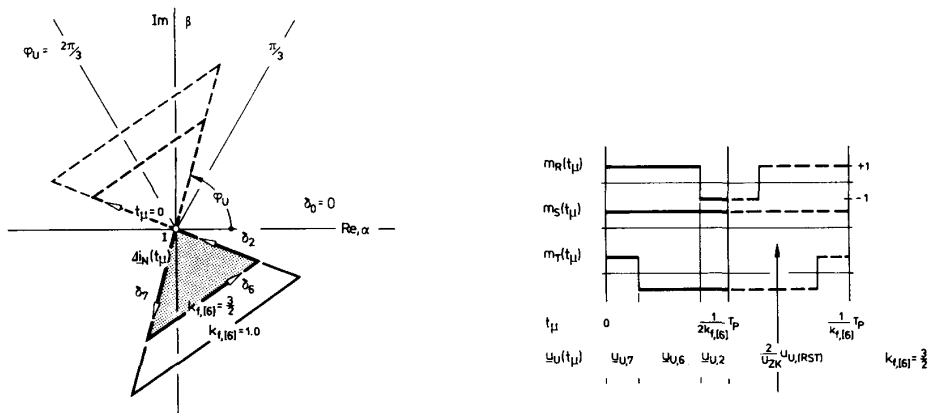


Fig.4: Trajectory of the space vector Δi_N of the current harmonics for a switching sequence according to Eq.(24) (modulation method [6]). There are conditions shown for the case of a pulse frequency equal as for continuous modulation and for the case of a pulse frequency increased by a factor of $k_{f,[i]} = \frac{3}{2}$; right side: microscopic time behavior of the related normalized converter phase voltages (for $k_{f,[i]} = \frac{3}{2}$); parameter: $M = 0.75$, $\varphi_U = 75^\circ$.

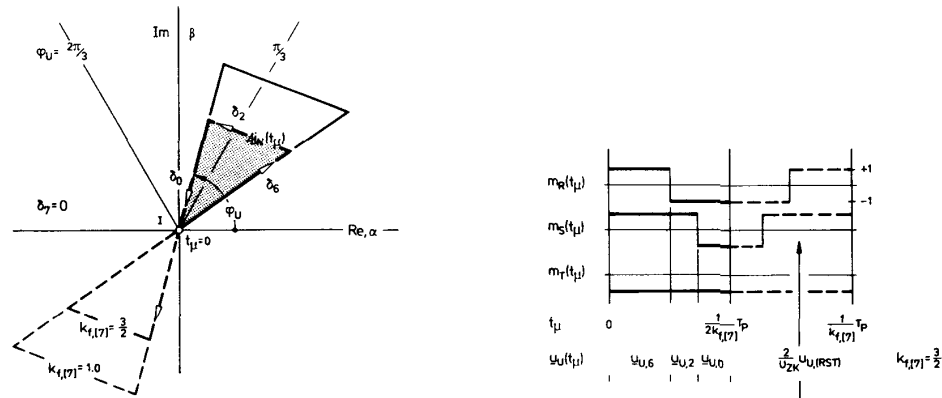


Fig.5: As Fig.4, but modulation method [7] (according to Eq.(25)).

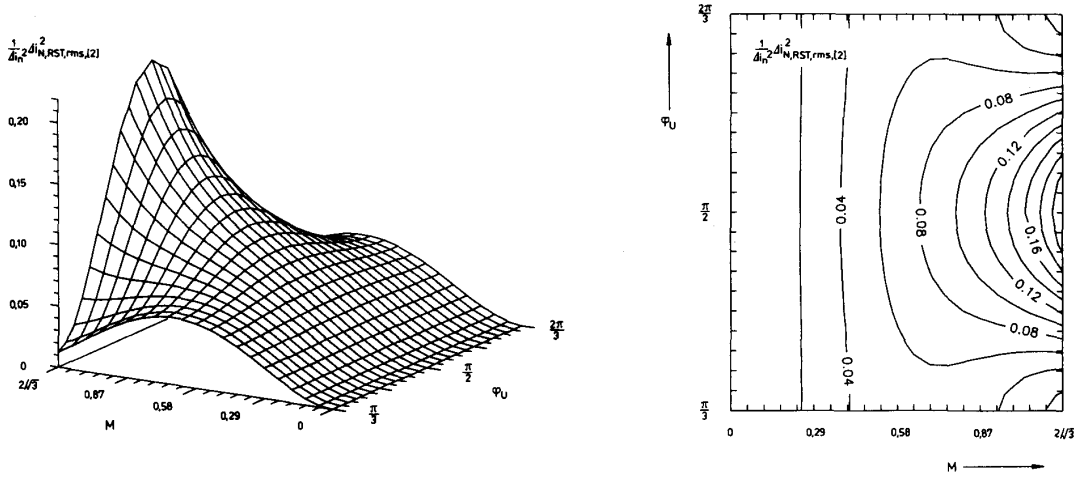


Fig. 6: Dependency of the normalised harmonic losses $\Delta i_{N,RST,rms,[2]}^2$ on the modulation index M and on the phase φ_U of the converter voltage space vector \underline{u}_U^* for modulation method [2] (continuous modulation).

position of the pulse interval φ_U for the (sub)optimal continuous modulation [2] (cf. Eqs.(8), (15), (16), (17) and (21)).

For characterising the local harmonic power loss contributions of the (discontinuous) modulation methods [6] and [7] there follow Figs.7 and 8 after introducing the defining equations

$$\varphi_U \in \left[\frac{\pi}{3}, \frac{2\pi}{3} \right] \quad \delta_{0,[6]} = 0 \quad \delta_{7,[6]} = 1 - (\delta_2 + \delta_6) \quad (27)$$

and

$$\varphi_U \in \left[\frac{\pi}{3}, \frac{2\pi}{3} \right] \quad \delta_{7,[7]} = 0 \quad \delta_{0,[7]} = 1 - (\delta_2 + \delta_6) \quad (28)$$

and considering Eqs.(8), (15), (16), (17). Due to the there not yet considered possibility of increasing the pulse frequency (as mentioned before, factor $k_{f,[i]}$) the local harmonic losses (cf. Figs.7 and 8) lie always above the approximation of the minimum surface as given for [2] (cf.Fig.6).

Figures 7 and 8 suggest the definition of a further discontinuous modulation method [4] by combining modulation methods [6] and [7] according to

$$\begin{aligned} \varphi_U \in \left[\frac{\pi}{3}, \frac{\pi}{2} \right] & \quad \delta_{0,[4]} = 0 & \quad \delta_{7,[4]} = 1 - (\delta_2 + \delta_6) \\ \varphi_U \in \left[\frac{\pi}{2}, \frac{2\pi}{3} \right] & \quad \delta_{7,[4]} = 0 & \quad \delta_{0,[4]} = 1 - (\delta_2 + \delta_6) \end{aligned} \quad (29)$$

(cf. Fig.9). According to the defining equation, in dependency on the position φ_U of the converter voltage phasor that particular modulation method is selected there which makes the smallest contribution to the global harmonic power losses. E.g., for $\varphi_U = 75^\circ$ and $M = 0.75$ (cf. Figs.7 and 8) modulation method [6] shows a distinctively lower harmonics power loss contribution as compared to modulation method [7]. This can be illustrated also by the different "moment of inertia" of the current harmonic triangles as shown in Figs.4 and 5.

Based on the explanations given, the (discontinuous) modulation method denoted by [5] and defined by the alternative combination

$$\begin{aligned} \varphi_U \in \left[\frac{\pi}{3}, \frac{\pi}{2} \right] & \quad \delta_{7,[5]} = 0 & \quad \delta_{0,[5]} = 1 - (\delta_2 + \delta_6) \\ \varphi_U \in \left[\frac{\pi}{2}, \frac{2\pi}{3} \right] & \quad \delta_{0,[5]} = 0 & \quad \delta_{7,[5]} = 1 - (\delta_2 + \delta_6) \end{aligned} \quad (30)$$

of modulation methods [6] and [7] does not seem to be very advantageous at first (cf. Figs.10 and 9). However, as shown in detail later, the admissible pulse frequency increase for [5] in wide operating regions lies substantially above the increase as possible for [4]. (The basis of comparison is given by maintaining the same average switching losses (related to the fundamental) as occurring for continuous modulation for pulse frequency f_P). This justifies an inclusion of modulation method [5] into further considerations.

After comparing the local harmonic power loss contributions of modulation methods [6], [7] and of the derived methods [4], [5] we will now calculate the harmonic power loss defining the actual quality index (or the harmonic current rms values related to the fundamental) of the different modulation methods, and compare the results.

The (normalised) harmonic power losses for continuous modulation have been given already in section 4. For discontinuous modulation there follow under consideration of the defining equations (Eqs.(27), (28), (29) and (30)) of the various modulation methods the relationships

$$\Delta I_{N,rms,[6]}^2 = \frac{1}{6} \Delta i_n^2 M^2 \frac{1}{k_{f,[6]}^2} \left[4 - \frac{35M}{\sqrt{3}\pi} + \frac{9M^2}{8} \left(2 + \frac{3\sqrt{3}}{4\pi} \right) \right] \quad (31)$$

$$\Delta I_{N,rms,[7]}^2 = \frac{1}{6} \Delta i_n^2 M^2 \frac{1}{k_{f,[7]}^2} \left[4 - \frac{35M}{\sqrt{3}\pi} + \frac{9M^2}{8} \left(2 + \frac{3\sqrt{3}}{4\pi} \right) \right] \quad (32)$$

$$\Delta I_{N,rms,[4]}^2 = \frac{1}{6} \Delta i_n^2 M^2 \frac{1}{k_{f,[4]}^2} \left[4 - \frac{M}{\sqrt{3}\pi} (62 - 15\sqrt{3}) + \frac{9M^2}{8} \left(2 + \frac{\sqrt{3}}{\pi} \right) \right] \quad (33)$$

and

$$\Delta I_{N,rms,[5]}^2 = \frac{1}{6} \Delta i_n^2 M^2 \frac{1}{k_{f,[5]}^2} \left[4 - \frac{M}{\sqrt{3}\pi} (8 + 15\sqrt{3}) + \frac{9M^2}{8} \left(2 + \frac{\sqrt{3}}{2\pi} \right) \right] \quad (34)$$

($k_{f,[i]}$ denotes, as mentioned, the possible frequency increase when discontinuous modulation [i] is applied as compared to applying continuous modulation [2] (cf.Eq.(26))).

Figure 11 shows graphically the relationships defined by Eqs.(23), (31), (32), (33) and (34). As one can expect, the harmonic power losses for discontinuous modulation lie in the whole modulation region above the values obtainable by continuous modulation (note: $k_{f,[i]} = 1!$).

For exclusive consideration of discontinuous modulation (as immediately clear by inspection of Figs.7,8,9,10) the modulation method [4] shows the lowest, the modulation method [5] the highest harmonic power losses. [6] and [7] lead to identical results (cf. Eqs.(31), (32) and the symmetry conditions of Figs.7 and 8) and lie between [4] and [5].

Finally, we want to mention that for all modulation methods treated here the maximum possible modulation range (limit to overmodulation) is given by

$$M \in \left[0, \frac{2}{\sqrt{3}} \right]. \quad (35)$$

This can be explained by the fact that discontinuous modulation only means that the distribution of the free-wheeling states is in a different manner as compared to continuous modulation. The distribution of the free-wheeling states does not influence the voltage space vector \underline{u}_U^* (cf. Fig.2) which is generated in the average over one pulse period, but it influences essentially the occurring current harmonics.

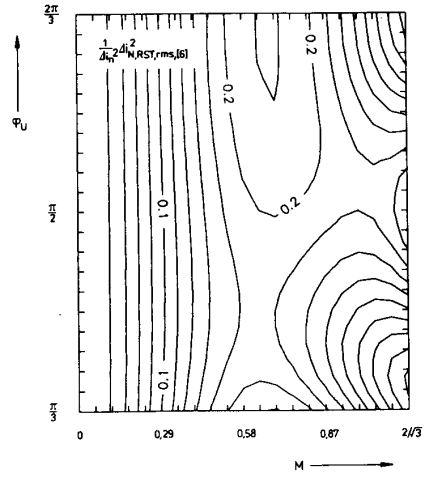
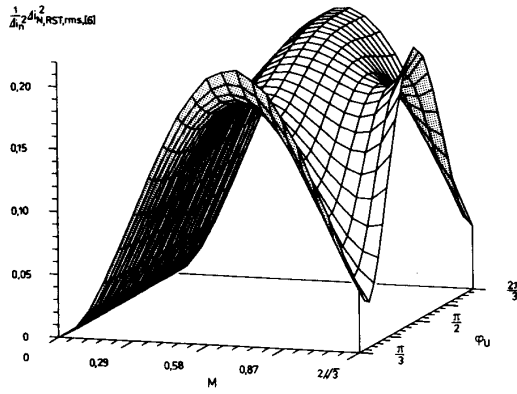


Fig.7: Dependency of the normalised local harmonic power losses $\Delta_{N,RST,rms,[6]}^2$ on the modulation index M and on the phase φ_U of the converter voltage space vector for modulation method [6] (discontinuous modulation); parameter: $k_{f,[6]} = 1!$

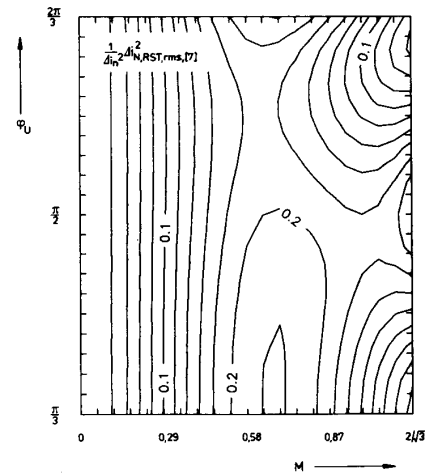
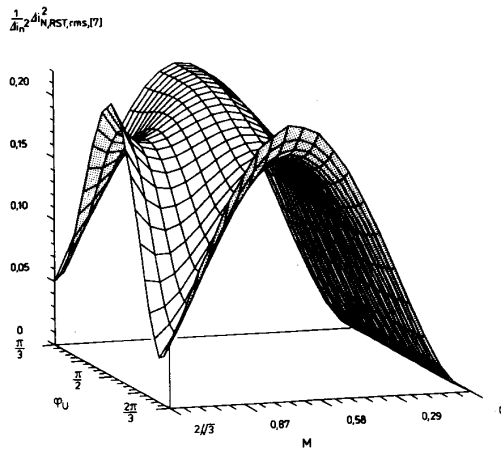


Fig.8: As Fig.7, but for modulation method [7]; parameter: $k_{f,[7]} = 1!$

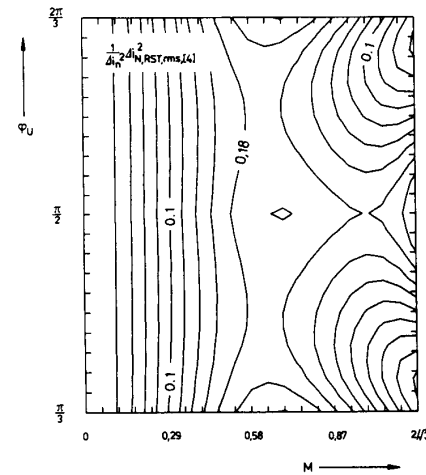
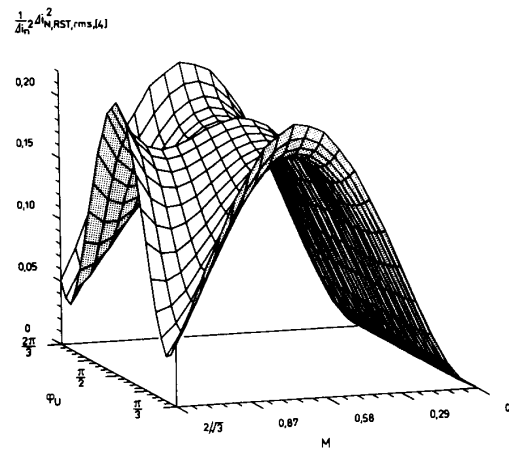


Fig.9: As Fig.7, but for modulation method [4]; parameter: $k_{f,[4]} = 1!$ Modulation method [4] follows from a combination of modulation methods [6] and [7] according to: [6]: $\varphi_U \in [\frac{\pi}{3}, \frac{\pi}{2}]$, [7]: $\varphi_U \in [\frac{\pi}{2}, \frac{2\pi}{3}]$.

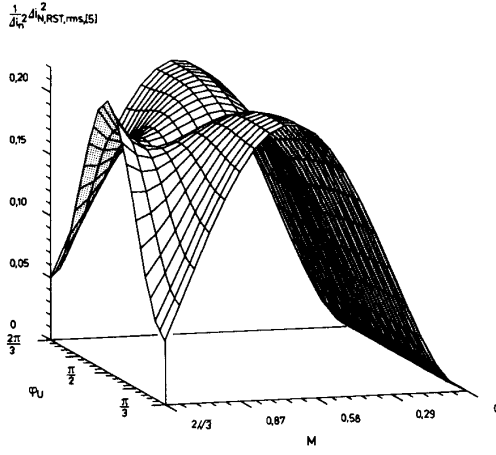


Fig.10: As Fig.7, but for modulation method [5]; parameter: $k_{f,[5]} = 1$! Modulation method [5] follows from a combination of modulation methods [6] and [7] according to: [7]: $\varphi_U \in [\frac{\pi}{3}, \frac{2\pi}{3}]$, [6]: $\varphi_U \in [\frac{\pi}{2}, \frac{2\pi}{3}]$.

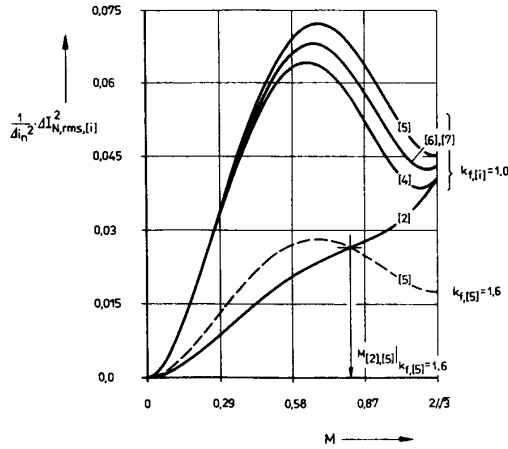
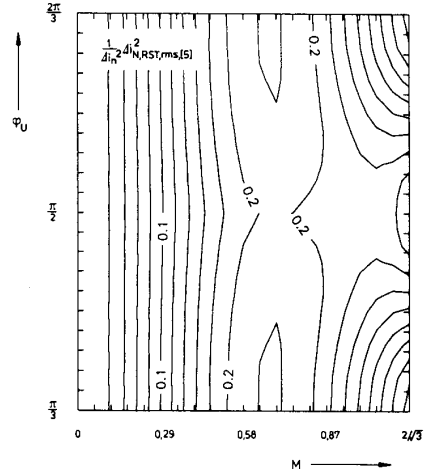


Fig.11: Comparison of the (global) current harmonic rms values for continuous modulation [2] and for discontinuous modulation [4-7] on the basis of $k_{f,[i]} = 1$. Under consideration of the increase of the effective pulse frequency which becomes possible for discontinuous modulation (cf. section 6) the discontinuous modulation methods (shown for the example of [5] for $k_{f,[5]} = 1.6$) show lower harmonic losses in the upper modulation region (for $M > M_{[2],[5]}$) than the continuous modulation [2].

6 Admissible Pulse Frequency Increase for Discontinuous Modulation

As shown in Refs.[1], [8] one can obtain the average (related to the fundamental) switching loss $P_{P,T2,D1}$ of a diode/transistor combination (T2 and D1, see phase R in Fig.1) for high pulse rates simply by integration of

$$P_{P,T2,D1} = \frac{1}{2\pi} \int_{-\pi/2-\varphi}^{+\pi/2-\varphi} p_{P,T2,D1}(\varphi_U) d(\varphi_U), \quad (36)$$

i.e., of the local power losses $p_{P,T2,D1}(\varphi_U)$. There, the integration has to be made over that interval within which the electric valves (e.g., T2 and D1) alternatively conduct the phase current. In the case at hand this means the half-period with positive current. The local power losses are defined according to

$$p_{P,T2,D1}(\varphi_U) = \frac{1}{T_P} w_{P,T2,D1}(\varphi_U) = f_P \cdot w_{P,T2,D1} \quad (37)$$

as switching energy loss weighted by the switching frequency. As experimentally verified, this energy loss shows approximately a linear dependency

$$w_{P,T2,D1}\{i_N(\varphi_U)\} = k_{1,TD} i_N(\varphi_U) \quad i_N(\varphi_U) \geq 0 \quad (38)$$

with the factor

$$k_{1,TD} = k_{1,T} + k_{1,D} \quad (39)$$

on the phase current $i_N(\varphi_U)$ to be switched locally at position φ_U . For continuous modulation there follows under the assumption of a purely sinusoidal phase current shape

$$P_{P,T2,D1} = \hat{I}_N f_P \frac{k_{1,TD}}{\pi} \quad (40)$$

If a converter bridge leg is switched only in certain segments (i.e., for discontinuous modulation; cf. section 5), there results a corresponding reduction of the averaged switching losses. Also, one can say that the effective pulse frequency of the converter can be increased for equal average switching losses as for continuous modulation.

Remark: Besides the switching losses also the local conduction losses are influenced for clamping of a bridge leg in certain time intervals. This is because within these intervals the current flows only through the transistor or the diode of one half of the converter bridge leg (and not through valves of different bridge leg halves). A more detailed analysis (Ref.[3]) shows no essential changes of the conduction losses averaged over the fundamental period, however. Therefore, in the following we do not want to consider this aspect. This is especially adequate here because we consider PWM converters with high switching frequency where mainly the switching losses determine the junction temperature.

The possible switching frequency increase is influenced by the duration

and distribution (or by the position) of the clamping intervals within the current fundamental (cf. Ref.[3]). The switching losses are reduced substantially if, e.g., for a given phase angle there exists a phase relationship between converter phase voltage and phase current such that the clamping intervals will lie in the vicinity of the current maxima. On the contrary, if the clamping intervals lie in the vicinity of the current zero crossings there results a smaller switching loss reduction and therefore a lower possible switching frequency increase. In summary, each discontinuous modulation method [i] shows a characteristic dependency of the possible switching frequency increase $k_{f,[i]}$ on the phase angle φ of the output current.

A detailed analysis (given in Ref.[3]) leads to

$$k_{f,[4]} = \frac{f_{P,[4]}}{f_P} = \begin{cases} \frac{1}{1 - \frac{(\sqrt{3}-1)}{2} \cos \varphi} & \varphi \in [0, \frac{\pi}{6}] \\ \frac{2}{\sin \varphi + \cos \varphi} & \varphi \in [\frac{\pi}{6}, \frac{\pi}{3}] \\ \frac{1}{1 - \frac{(\sqrt{3}-1)}{2} \sin \varphi} & \varphi \in [\frac{\pi}{3}, \frac{\pi}{2}] \end{cases}, \quad (41)$$

$$k_{f,[5]} = \frac{f_{P,[5]}}{f_P} = \begin{cases} \frac{1}{(1 - \frac{1}{2} \cos \varphi)} & \varphi \in [0, \frac{\pi}{3}] \\ \frac{2}{\sqrt{3} \sin \varphi} & \varphi \in [\frac{\pi}{3}, \frac{\pi}{2}] \end{cases}, \quad (42)$$

$$k_{f,[6]}(\varphi) = k_{f,[5]}(\varphi - \frac{\pi}{6}) \quad (43)$$

and

$$k_{f,[7]}(\varphi) = k_{f,[5]}(\varphi + \frac{\pi}{6}). \quad (44)$$

Values for the other phase angle regions follow by symmetry considerations (cf. Fig. 12).

As can be seen from Fig.12, one can achieve twice the effective pulse frequency (clamping is performed symmetrically with respect to the positive and negative maxima of the phase current, cf. Ref.[3]) for selected phase angles using modulation methods [5], [6] and [7]. This also results in a harmonic loss reduction by a factor of $1/k_f^2 = \frac{1}{4}$ as compared to $k_f = 1$ (cf. Eqs.(31),(32),(33),(34)). The modulation method [4] (cf. Fig.11) showing the smallest harmonic power losses (as achievable by discontinuous modulation) for $k_f = 1$ allows only a pulse frequency increase by 50%, but for the whole phase angle region.

Now the question arises which modulation method will result in the smallest harmonic power losses for given modulation index and phase angle, or, where a transition between continuous modulation and discontinuous modulation has to be made.

7 Transition from Continuous Modulation to Discontinuous Modulation

The calculation of that modulation index $M_{[2],[i]}$ from which on (for given $k_{f,[i]}$) the harmonic power losses $\Delta I_{N,rms,[i]}^2$ of the discontinuous modulation method [i] are decreased below the losses for continuous modulation can simply be performed by solving the resulting quadratic equations

$$\frac{9M_{[2],[5]}^2}{8} \left[\frac{3\sqrt{3}}{4\pi} - 1 + \frac{1}{k_{f,[5]}^2} (2 + \frac{\sqrt{3}}{2\pi}) \right] + \frac{M_{[2],[5]}}{\sqrt{3}\pi} \left[8 - \frac{1}{k_{f,[5]}^2} (8 + 15\sqrt{3}) \right] - (1 - \frac{4}{k_{f,[5]}^2}) = 0 \quad (45)$$

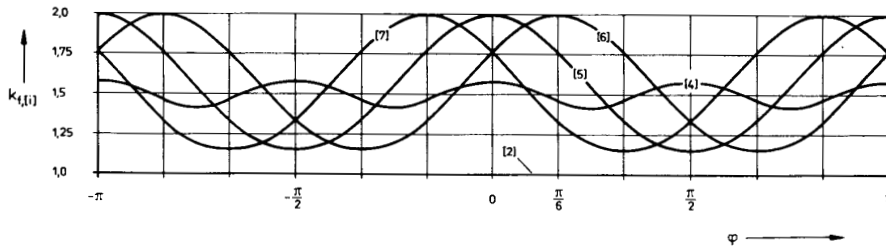


Fig.12: Dependency of the possible frequency increase $k_{f,[i]}$ on the phase angle φ between converter phase voltage and phase current (cf. Eqs.(41), (42), (43), (44)) for discontinuous modulation [i] (related to continuous modulation with equal average switching power loss).

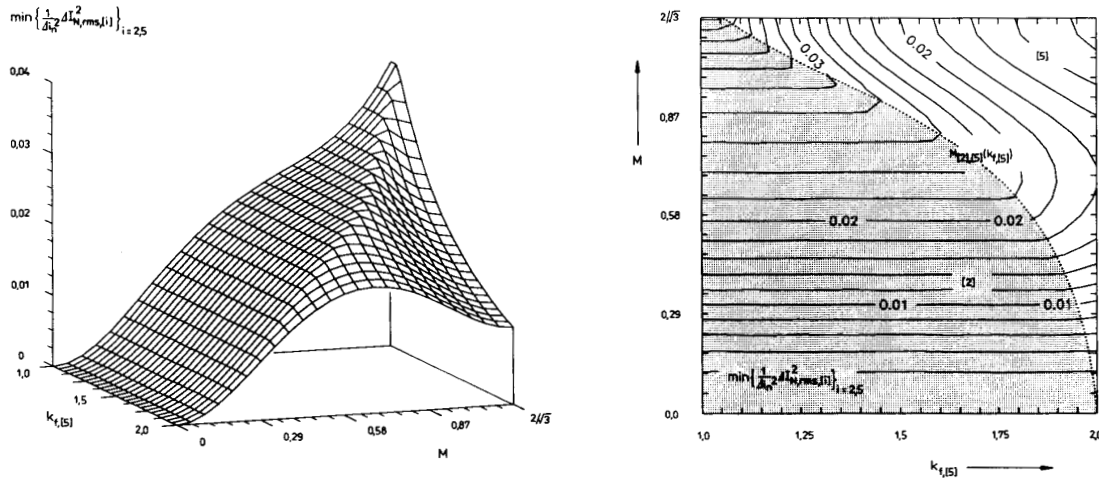


Fig.13: Dependency of the minimum $\min \left\{ \frac{1}{\Delta t^2} \Delta I_{N,rms,[i]}^2 \right\}$ of the normalized harmonic power losses of continuous modulation [2] and of discontinuous modulation [5] on the frequency increase $k_{f,[5]}$. In the topographical representation (right hand side) the region of continuous modulation [2] is pointed out by the dotted area.

(given for modulation method [5]; the other equations are analogous, cf. Eq.(23) and Eqs.(31), (32), (33)).

The combination of modulation methods [2] and [5] in dependency on $k_{f,[5]}$ is shown in Fig.13. For $k_{f,[5]} = 2$ the harmonic power losses of the discontinuous modulation lie below the losses of the continuous modulation in the whole modulation region.

For a given phase angle, we can calculate the respective value $k_{f,[i]}$ for each modulation method by using Eqs.(41), (42), (43), (44). In a further step, we can determine the intersections $M_{[2],[i]}$ (Eq.(45); cf. also Fig.14)). Therefore, there follow directly these phase-angles/modulation-regions where continuous modulation [2] leads to the lowest harmonic power loss (pointed out in Fig.14 by the dotted area).

8 Harmonic-Optimal Combination of Continuous and Discontinuous Modulation

Because in the previous section only the transition from continuous modulation to discontinuous modulation has been treated, we now want to investigate in conclusion which modulation method ([2], [4], [5], [6] or [7]) results in the lowest harmonic power losses for given modulation index and phase angle. We also will show the dependency on the respective operating condition. The minimum area of the harmonic power losses resulting by using Eqs.(23), (31), (32), (33), (34), (41), (42), (43), (44) is shown in Fig.15. We want to mention that the optimal transition between the modulation methods regarding the

possible frequency increase or regarding the effective system pulse frequency is not continuous.

Basically, therefore one has to change from continuous to discontinuous modulation in the upper modulation region. The discontinuous modulation method to be applied is essentially determined by the given phase angle φ or by the frequency increase ($k_{f,[i]}(\varphi)$, cf. Fig.12) possible there. As a simple suboptimal approximation of the harmonics power loss optimal transition strategy (defined by the dotted boundary lines in Fig.15, right hand side) therefore one always has to apply that discontinuous modulation method which allows the maximum frequency increase.

In general, there follow different harmonic optimal modulation methods for each specific application of the PWM converter system. For application as PWM rectifier we have high modulation indices and phase angles close to 0. The harmonic optimal modulation method is given by [5]. For operation of the converter as static Var compensator we have a phase angle close to $\pm \frac{\pi}{2}$ and also high modulation indices. Accordingly, we then have to apply modulation method [4]. For machine converters we have a comparatively wide phase angle and modulation index region ($\varphi \approx \in \pm [\frac{\pi}{6}, \frac{\pi}{2}]$). Furthermore, we then have to consider the dependency of the current amplitude on the phase angle (note that the comparison of the modulation methods has been performed for phase-angle-independent current amplitude, cf. Eq.(40)) and a thermal limitation of the discontinuous modulation (cf. remark regarding the thermal inertia of power electronic devices in section 9). Also, in this case, the discontinuous modulation (modulation methods [6] and [7]) shows significant advantages in the upper speed range as compared to continuous modulation [2]. Therefore, the discontinuous modulation has to be included

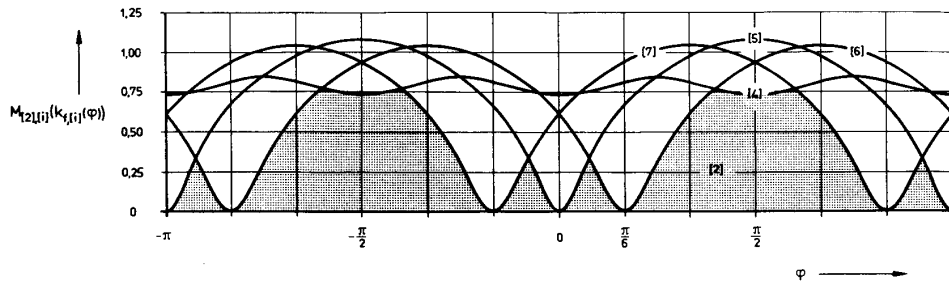


Fig.14: Illustration of the determination of the limit between continuous modulation [2] and discontinuous modulation [4]-[7] in dependency on the phase angle; region of continuous modulation [2] pointed out by the dotted area.

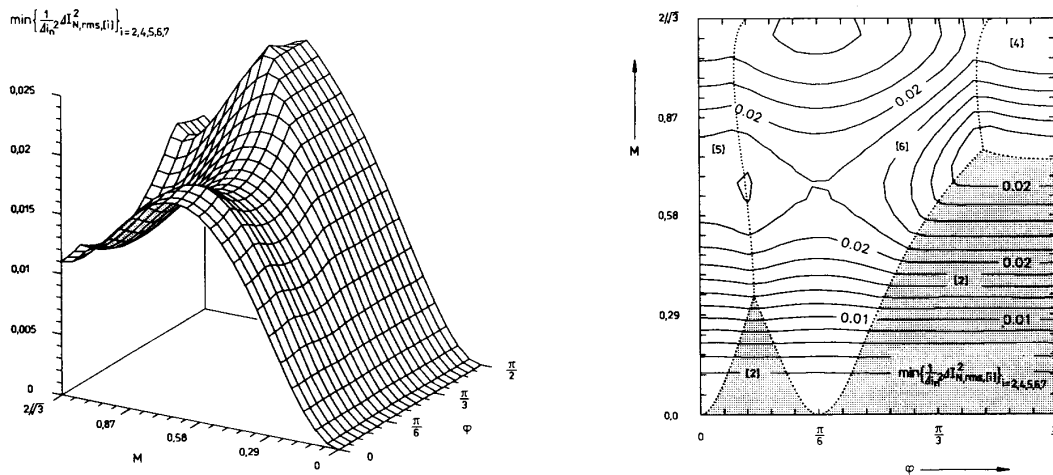


Fig.15: Dependency of the normalized harmonic power losses on the phase angle φ and on the modulation index M for harmonics power loss optimal combination of continuous modulation [2] and discontinuous modulation [4], [5], [6] or [7]. The representation is limited to $\varphi \in [0, \frac{\pi}{2}]$. The other regions follow by considering Figs.12 and 14 using simple symmetry considerations (note especially [6] and [7] in Fig.14). One can clearly recognise the application limits of the different modulation methods as pointed out in the topographical representation. The region of continuous modulation [2] has been pointed out again (as in Figs.13 and 14) by the dotted area.

into the choice of the modulation method in any case.

Basically, there would be a frequency increase by a factor of $k_f = 2$ for the entire phase angle region $\varphi \in [-\frac{\pi}{6}, +\frac{\pi}{6}]$ possible using discontinuous modulation. (Therefore, an even greater reduction of the harmonic power loss would be achieved.) However, then the clamping region (being symmetrical to the current maximum for $\varphi = 0$) of the discontinuous modulation [5] would have to be shifted according to the phase angle (or to the current maximum). [5] then coincides with [6] for $\varphi = +\frac{\pi}{6}$ and with [7] for $\varphi = -\frac{\pi}{6}$ (cf. Fig.12).

9 Conclusions

As mentioned, we have assumed a sufficiently high converter pulse rate pz for the calculations made. A comparison (not given in detail here) of the approximate calculation and of a digital simulation shows already for $pz \geq 21$ excellent consistency of the results (maximum deviation $< 1\%$). The assumption of high pulse rates therefore does not mean a basic limitation of the considerations given in this paper. This is especially true because modern power electronic devices allow relatively high switching rates.

Regarding the comparison of continuous and discontinuous modulation (which is based on equal average switching power loss, related to the fundamental period) we have to note that this implies a sufficiently high thermal inertia of the power electronic devices. Only then the local power loss shape results in an only marginally changing junction temperature, which is determined by the power loss average and which can be used for a thermal dimensioning of the power semiconductors. For low output frequencies (e.g., for supplying AC machines in the lower speed/modulation region) or for low thermal inertia of the valves, the maximum junction temperature is determined directly by the local power loss shape. Then the comparison of different modulation methods becomes much more complicated. For a specific application of the results derived in this paper therefore one has to check the time dependency of the junction temperature. This can be done, e.g., by approximating the transient thermal resistance by a thermal equivalent circuit of second order and by using the local switching and conduction losses. A calculation to check the conditions for mains operation of a converter system consisting of 100A/1200V IGBT half-bridge modules shows that the assumptions made in this paper are sufficiently well met. In this case we have operation with high modulation indices and therefore discontinuous modulation (cf. Fig.15); the details of this calculation have to be omitted here for the sake of brevity. The thermal limitation of the discontinuous modulation (to be inserted into Fig.15) for application as modulation method for drives with high speed range will be the topic of a future paper being under preparation.

Specific methods of discontinuous modulation methods given in the literature (see Refs.[9], [10], [11], [12], [13]) which can be derived as subsets of the modulation methods treated here do not consider the "thermal side condition" and are based on a possible frequency increase by a factor of $k_f = \frac{3}{2}$. The possible frequency increase there is only derived from the lower number of switchings per pulse half-period for discontinuous modulation (2 instead of 3 switchings as used for continuous modulation). There it is not taken into account where (i.e. for which current) the switch occurs. The actually possible frequency increase for these modulation methods will be also the topic of a future paper.

We have to note that also for classical pulse pattern optimization (cf. e.g., Refs.[14], [15]) the actual thermal conditions of the power electronic devices remain unconsidered. There, a given quality index is optimised by appropriate shifting of a given number of switching angles per fundamental quarter period. Therefore, the thermal stress on the power electronic devices is changed during the course of the optimisation. This aspect is especially of interest if the pulse pattern shows clamping intervals (cf. Ref.[15]); this can lead to a reduction of the switching losses (as for discontinuous modulation) and, alternatively to a higher admissible number of switching angles. A closer analysis of these aspects (which have not been discussed in literature so far) would be certainly of interest. However, the computational effort probably is very high because already without considering these aspects computing times are tremendous for a higher given number of switching angles.

A comparison of the solutions presented here with the classical pulse pattern optimisation shows in general that also there (i.e., already for a relatively low number of switching angles) in the case of a loss minimisation (cf. EOC in Ref.[15]) two classes of solutions can be observed. They correspond basically to the continuous and to the discontinuous modulation as can be seen by comparing the dependencies of the normalised harmonic power losses on the converter modulation index (cf. Fig.11).

In conclusion, we want to point out that (as shown in Ref.[16] and as mentioned also in Ref.[13]) all the considerations described in this paper also

can be applied to converters with DC current link if one applies the duality relations. Due to the very clear representation of the system quantities by space vectors and due to the implicate decoupling of zero quantities also in this case this method has to be highly preferred as compared to using phase quantities. A more detailed discussion shall be omitted here for the sake of brevity.

References

- [1] Kolar, J. W., Ertl, H., and Zach, F. C.: *Calculation of the Passive and Active Component Stress of Three-Phase PWM Converter Systems with High Pulse Rate*. Proceedings of the 3rd European Conference on Power Electronics and Applications, Aachen, Oct. 9-12, Vol. 3, 1303-1311 (1989).
- [2] Kolar, J. W., Ertl, H., and Zach, F. C.: *Analytically Closed Optimization of the Control Method of a PWM Rectifier System with High Pulse Rate*. Proceedings of the PCIM'90, Munich, June 27-29 (1990).
- [3] Kolar, J. W., Ertl, H., and Zach, F. C.: *Influence of the Modulation Method on the Conduction and Switching Losses of a PWM Converter System*. Conference Record of the 25th IEEE IAS Annual Meeting, Seattle, Oct. 7-12, Pt.I, 502-512 (1990).
- [4] van der Broeck, H. W., Skudelny, H. C., and Stanke, G. V.: *Analysis and Realization of a Pulsewidth Modulator Based on Voltage Space Vectors*. IEEE Transactions on Industry Applications, Vol. IA-24, No.1, 142-150 (1988).
- [5] Kolar, J. W., Ertl, H., and Zach, F. C.: *Minimization of the Harmonic RMS Content of the Mains Current of a PWM Converter System Based on the Solution of an Extreme Value Problem*. Proceedings of the ICHPS IV, Budapest, Oct. 4-6, 234-243. (1990).
- [6] Bowes, S. R., and Midoun, A.: *Suboptimal Switching Strategies for Microprocessor-Controlled PWM Inverter Drives*. IEE Proceedings, Vol. 132, Pt. B, No. 3, 133-148 (1985).
- [7] Buja, G., and Indri, G.: *Improvement of Pulse Width Modulation Techniques*. Archiv für Elektrotechnik 57, 281-289 (1977).
- [8] Ikeda, Y., Itsumi, J., and Funato, H.: *The Power Loss of the PWM Voltage-Fed Inverter*. Record of the 19th PESC, Kyoto, Japan, April 11-14, Vol.1, 277-283 (1988).
- [9] Taniguchi, K., Ogino, Y., and Irie, H.: *PWM Technique for Power MOSFET Inverter*. IEEE Transactions on Power Electronics, Vol.3, No.3, 328-334 (1988).
- [10] Fukuda, S., Hasegawa, H., and Iwaji, Y.: *PWM Technique for Inverter with Sinusoidal Output Current*. Record of the 19th IEEE PESC, Kyoto, Japan, April 11-14, Vol.1, 35-41 (1988).
- [11] Ogasawara, S., Akagi, H., and Nabae, A.: *A Novel PWM Scheme of Voltage Source Inverters Based on Space Vector Theory*. Proceedings of the 3rd European Conference on Power Electronics and Applications, Aachen, Oct. 9-12, Vol. 3, 1197-1202 (1989).
- [12] Taniguchi, K.: *Sinusoidal PAM-PWM Inverter Using Power MOSFETS*. Proceedings of the 3rd European Conference on Power Electronics and Applications, Aachen, Oct. 9-12, Vol. 2, 633-637 (1989).
- [13] Ziogas, P. D., Moran, L., Joos, G., and Vincenti, D.: *A Refined PWM Scheme for Voltage and Current Source Converters*. Conference Record of the 25th IEEE IAS Annual Meeting, Seattle, Oct. 7-12, Pt.II, 977-983 (1990).
- [14] Patel, H. S., and Hoft, R. G.: *Generalized Technique of Harmonic Elimination and Voltage Control in Thyristor Inverters: Part I - Harmonic Elimination*. IEEE Transactions on Industry Applications, Vol.IA-9, No.3, 310-317 (1973).
- [15] Zach, F. C., and Ertl, H.: *Efficiency Optimal Control for AC Drives with PWM Inverters*. IEEE Transactions on Industry Applications, Vol. IA-21, No. 4, 987-1000 (1985).
- [16] Kolar, J. W., Ertl, H., und Zach, F. C.: *Analysis and Duality of Three-Phase Converters with DC Voltage Link and DC Current Link*. Conference Record of the 24th Industry Applications Society Annual Meeting, San Diego, 1.-5. Oktober, Vol. 1, 724-737 (1989).